Supermicroporous niobium oxide as an acid catalyst

Mayako Hiyoshi[1], Byongjin Lee[1,4], Daling Lu[3], Michikazu Hara[1], Junko N. Kondo[1], and Kazunari Domen[2,3,*]

[1]*Chemical Resources Laboratory, Tokyo Institute of Technology, 4259 Nagatsuta-cho, Midori-ku, Yokohama 226-8503, Japan*
[2]*Department of Chemical System Engineering, School of Engineering, The University of Tokyo, 7-3-1 Hongo, Bunkyo-ku, Tokyo 113-8656, Japan*
[3]*CREST (Core Research for Evolutional Science and Technology) of JST (Japan Science and Technology)*
[4]*Present address:Samsung Fine Chemicals, Co. LTD., 103-1, Moonji-dong, Yoosung-gu, Daejeon 305–380, Korea*

Received 3 May 2004; accepted 20 September 2004

Supermicroporous (1.5–2.5 nm pore diameter) niobium oxide is synthesized using a nonionic block copolymer as a structural directing reagent, which is removed by water washing after aging. The oxide contains water in the bulk material in the form of a water-rich niobium oxide. The supermicroporous niobium oxide is applicable for various acid-catalyzed reactions.

KEY WORDS: catalytic activity; microporous material; niobium oxide; sol-gel method; solid acid catalyst.

1. Introduction

Hydrated niobium pentoxide (niobic acid, $Nb_2O_5 \cdot nH_2O$) exhibits catalytic activity for various acid-catalyzed reactions, such as esterification of ethyl alcohol with acetic acid [1], hydrolysis of phenyloxirane [2], hydration of ethylene [3], and the Prins reaction [4]. The stable acidity of hydrated niobium pentoxide, even in the presence of water, makes the material attractive for industrial use as a heterogeneous catalyst. This property is also highly important for establishing less expensive and environmentally clean processes, particularly for acid-catalyzed reactions in which water molecules participate or are liberated [5].

Recently, the present authors reported the preparation of mesoporous [6] and supermicroporous (1.5–2.5 nm pore diameter) [7] niobium oxides with highly ordered porous structures and amorphous pore walls. Supermicroporous niobium oxide is prepared by applying a water washing procedure for template removal instead of generally used thermal treatment [7], as has been necessary for template removal in the common preparation of porous materials using block copolymer templates and metal chlorides [8,9].

This paper briefly reports on the preparation of supermicroporous niobium oxide and its catalytic activity evaluated by dehydration of 2-propanol and esterification of acetic acid with ethanol in gas and liquid phase.

2. Experimental

2.1. Materials

A triblock copolymer $HO(CH_2CH_2O)_{26}(CH_2CH(CH_3)O)_{39}(CH_2CH_2O)_{26}H$ (Pluronic P-85, Adeka Co.) was used as a neutral templating agent for organizing the metal oxide species. Niobium pentachloride (99.9%, Kojundo Chemical Lab. Co.) was used as the niobium source. Commercial $Nb_2O_5 \cdot nH_2O$ (AD-382, CBMM) was used as a reference hydrated niobium pentoxide acid catalyst.

2.2. Sample preparation

The samples were synthesized according to the method reported previously [7]. Briefly, 0.010 mol of $NbCl_5$ was added to 10 wt% P-85 propanol solution and stirred for 30–60 min. After the addition of 1 mL of 0.05 M NaCl aqueous solution, the sol solution was aged at 40 °C in air for 1 week to obtain template-containing niobium oxide or hydroxide gel. In order to stabilize the inorganic network for water washing, the gel samples were further aged at 100 °C for 1 day. The porous structure was formed by removal of the template from the aged gel by water washing. The gel was washed with 1.0–2.0 L of distilled water per gram of gel, and the washed samples were dried in air overnight at room temperature.

2.3. Characterization

Porous niobium oxides were characterized by X-ray diffraction (XRD), nitrogen adsorption–desorption measurements, transmission electron microscopy (TEM), elemental analysis, thermogravimetric and differential thermal analysis (TG/DTA). XRD patterns were measured using a Rigaku RINT 2100 diffractometer with Cu Kα radiation. Nitrogen gas adsorption–desorption isotherms were recorded using a Coulter SA-3100 system. For the Barrett–Joyner–Halenda (BJH) analysis [10], the pore-size distribution was obtained from the adsorption branch of the isotherms. The TEM images were observed using a 200 kV JEOL JEM2010F. Elemental analysis of

*To whom correspondence should be addressed.

1011-372X/04/1200–0181/0 © 2004 Plenum Publishing Corporation

carbon, hydrogen and nitrogen was performed on a LECO CHN-932 analyzer, and chloride was analyzed using a Yanaco SX-Elements Micro Analyzer YS-10. TG/DTA measurements were carried out using a Shimadzu DTG-50 instrument in air at a heating rate of 3 °C min^{-1}.

The acidic properties of the samples were evaluated by the indicator adsorption method and the temperature-programmed desorption (TPD) of ammonia. Dicinnamalacetone (p*K*a = −3.0), chalcone (p*K*a = −5.6), anthraquinone (p*K*a = −8.2) and *p*-nitorotoluene (p*K*a = −11.35) were used as basic indicators. The samples pretreated in vacuum at 80 °C were suspended in dry benzene solution of the indicator, and the change of the indicator color was observed to estimate the p*K*a values. The TPD of adsorbed ammonia was measured using a TPD-1-AT, BEL Japan, equipped with a quadrupole mass spectrometer. For TPD, a 0.020 mg sample was held with quartz wool in a quartz tube and pretreated at 150–300 °C under helium flow for l h. The sample was then exposed to ammonia at 100 °C for adsorption. TPD measurements were performed between 100 and 600 °C with a heating rate of 10 °C min^{-1} under helium flow.

2.4. Catalytic reactions

2.4.1. Dehydration of 2-propanol

Dehydration of 2-propanol was carried out as a test reaction for acid catalysis. A fixed-bed flow reactor was used under atmospheric pressure. The catalysts (0.2 g) were activated at either 200 or 250 °C under flow nitrogen (30 mL min^{-1}) for 1 h. The 2-propanol was then fed into the reactor (0.033 mL min^{-1}) mixed with the nitrogen flow (35 mL min^{-1}). The reaction was carried out for 4 h. The products were analyzed by gas chromatography (GC-12A, Shimadzu) with a PolapacQ (Waters Co.) column.

2.4.2. Liquid-phase esterification of acetic acid with ethanol

Liquid-phase esterification was carried out in a two-neck flask equipped with a water-cooler condenser. Ethanol (58.8 mL, 1 mol) and acetic acid (6 mL, 0.1 mol) were reacted over the catalyst (0.2 g) at 70 °C. The catalyst was activated in vacuum either at 200 or 250 °C, followed by reaction for 6 h. The products were analyzed by gas chromatography/mass spectrometry (GCMS-QP5050, Shimadzu) using a capillary column (DB-FF AP, Agilent Tech.).

2.4.3. Gas-phase esterification of acetic acid with ethanol

Gas-phase esterification of acetic acid with ethanol was carried out at 160 °C, the optimum reaction temperature reported in the literature [1], using a fixed-bed flow reactor. The catalyst (0.2 g) was pretreated at either 160 or 200 °C under nitrogen flow at 30 mL min^{-1} for 1 h. The flow rate of acetic acid with ethanol (volume ratio = 1:1) was. 0.033 mL min^{-1}. The reactants were fed into the reactor with nitrogen (40 mL min^{-1}). The reaction was carried out for 4 h and the products were analyzed by gas chromatography (GC-12A, Shimadzu) with a PolapacQ (Waters Co.) column.

3. Result and Discussion

3.1. Characterization of supermicroporous niobium oxide

Direct water washing of the as-synthesized sample causes the porous structure to collapse as observed in the XRD patern in figure 1a. This is most probably due to incomplete formation of the niobium oxide network. To solve this problem, the as-synthesized sample was aged in a second step at 100 °C for 1 day. Then, an XRD peak at around 1.5 °C appeared (figure lb), where the *d* value corresponds to 5.0–6.0 nm. The extent of template removal was confirmed by elemental analysis of carbon and chloride. The carbon and chloride contents were estimated to be less than 0.1% after template removal by water washing, compared to ca. 24% and 6%, respectively, in the sample before template removal (table 1). However, the washed sample contained considerably larger amounts of hydrogen. Complete removal of carbon and chloride was confirmed for the sample after template removal by calcination at 450 °C for 5 h, yet the sample treated in this way contained about a quarter of the hydrogen of the washed sample. This reflects the hydrated property of the supermicroporous oxide, as also evidenced by TG–DTA (below).

The porosity of supermicroporous niobium oxide has been reported previously [7] and is briefly summarized in table 2 for comparison with calcined samples. The washed and calcined samples both exhibit almost the

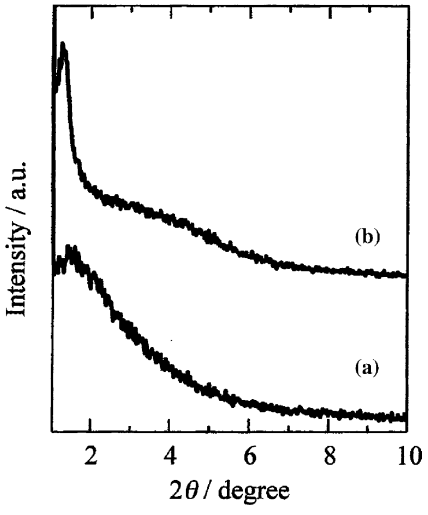

Figure 1. XRD patterns of supermicroporous niobium oxides, which were water-washed after aging at 40 °C (a) and 2nd step aging at 100 °C (b).

Table 1
Elemental analyses of porous niobium oxides*

Sample	Carbon/wt%	Hydrogen/wt%	Chloride/wt%
As-synthesized	23.9	5.1	5.9
Water-washed	0.1	2.2	>0.1
Calcined (450 °C, 5 h)	~0.0	0.6	~0.0

Table 2
Textural properties of porous niobium oxides

Sample	Pore size/nm	Pore volume/ml g^{-1}	BET surface area/m^2 g^{-1}
Water-washed	1.5–2.0	0.41	363
Calcined(450 °C, 5 h)	5	0.42	211

same pore volume, although the pore sizes are clearly different. This implies that mesopores in the calcined sample are formed by expansion of the supermicropores present in the as-prepared sample during the calcination process. A typical TEM image of supermicroporous niobium oxide is shown in figure 2, where the presence of supermicropores is confirmed for water-washed samples after second-step aging at 100 °C.

TG/DTA curves for $Nb_2O_5{\cdot}nH_2O$, supermicroporous and mesoporous niobium oxides are shown in figure 3. The DTA curve of $Nb_2O_5{\cdot}nH_2O$ has two endothermic peaks, at around 60 and 110 °C (figure 3a). The decrease in gravity continues to ca. 250 °C, and is considered to originate from the dehydration of $Nb_2O_5{\cdot}nH_2O$. The weight loss and DTA results for supermicroporous niobium oxide (figure 3b) are very similar to those of $Nb_2O_5{\cdot}nH_2O$, demonstrating the hydrated nature of the supermicroporous niobium oxide. On the other hand, the DTA curve for mesoporous niobium oxide does not exhibit a clear endothermic peak, with only a minor decrease in gravity (figure 3c). Thus, mesoporous niobium oxide is only slightly hydrated, This is understandable because mesoporous

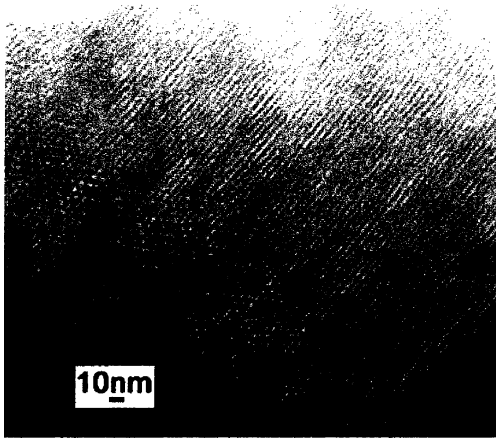

Figure 2. TEM image of supermicroporous niobium oxide obtained by template removal by water washing after 2nd step aging at 100 °C.

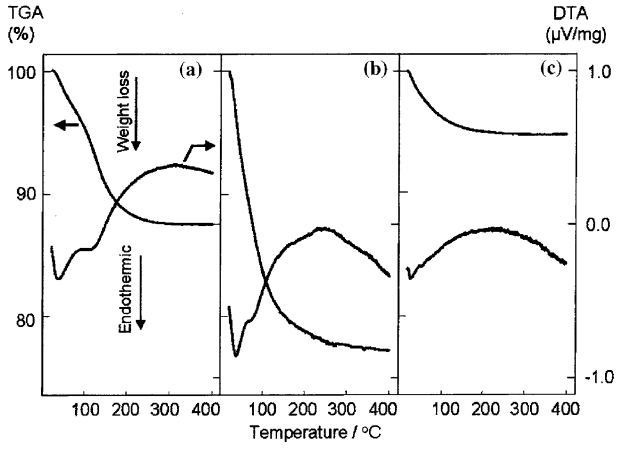

Figure 3. TG/DTA of $Nb_2O_5{\cdot}nH_2O$ (a), supermicroporous niobium oxide (b), and mesoporous niobium oxide (c).

niobium oxide is calcined at 450 °C, which would induce almost complete dehydration.

3.2. Acidity of supermicroporous niobium oxide

The color of supermicroporous niobium oxide changed in a solution of dicinnamalacetone (pKa = −3.0), chalcone (pKa = −5.6) and anthraquinone (pKa = −8.2), indicating that the acidity of supermicroporous niobium oxide corresponds to 90% sulfuric acid. The coloration results for $Nb_2O_5{\cdot}nH_2O$and mesoporous niobium oxide were the same, and as such the acidities of these samples are expected to be equal.

Figure 4 shows the NH_3-TPD (m/e = 16) spectra for adsorption onto catalysts treated at 200 °C. While two peaks, at around 180 and 280 °C are observed for all samples, the desorption peak at around 280 °C is more prominent for super microporous niobium oxide than the other niobium oxide samples. The difference between the integrated intensities of the supermicroporous and mesoporous samples is considered to reflect the hydrated properties of the former, that is, the species

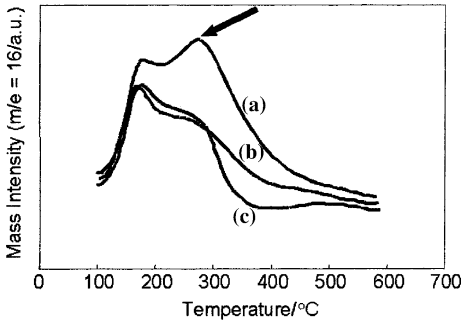

Figure 4. TPD spectra of NH_3 adsorbed on the catalysts treated at 200 °C: supermicroporous niobium oxide (a), $Nb_2O_5{\cdot}nH_2O$ (b) and mesoporous niobium oxide (c). The arrow indicates NH_3 desorption from strongly acidic sites, which is ecident for supermicroporous miobium oxide.

that desorb along with water as shown in figure 3 are responsible for the acidity. Moreover, the integrated mass intensity of the 280 °C peak for supermicroporous niobium oxide is larger than that for $Nb_2O_5{\cdot}nH_2O$, indicative of a higher density of acidic sites in supermicroporous niobium oxide. Therefore, supermicroporous niobium oxide can be expected to exhibit higher reactivity than $Nb_2O_5{\cdot}nH_2O$.

Figure 5 shows the NH_3- TPD (m/e = 16) results for supermicroporous niobium oxide catalysts treated at various temperatures. The catalyst pretreated at 200 °C exhibits a clear NH_3 desorption peak at 280 °C, whereas the samples pretreated at higher than 250 °C exhibit a progressively weaker peak. This behavior was also observed for $Nb_2O_5{\cdot}nH_2O$. As the TG/DTA curve shows that dehydration is complete at about 250 °C, the acid strength and amount supermicroporous niobium oxide are confirmed to be related to the amount of water in the bulk.

3.3. Catalytic reactions of supermicroporous niobium oxide

3.3.1. Dehydration of 2-propanol

Figure 6 compares the catalytic activities of supermicroporous and $Nb_2O_5{\cdot}nH_2O$. in the dehydration of 2-propanol. The reactions were performed at 200 and 250 °C after pretreatment at the same temperatures. At the reaction temperature of 200 °C, the yield of propene over supermicroporous niobium oxide is about twice

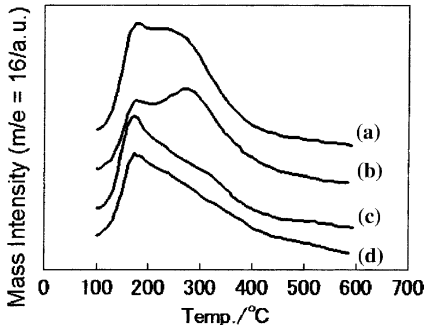

Figure 5. NH_3-TPD of supermicroporous niobium oxide treated at 150 °C (a), 200 °C (b), 250 °C (c), 300 °C (d).

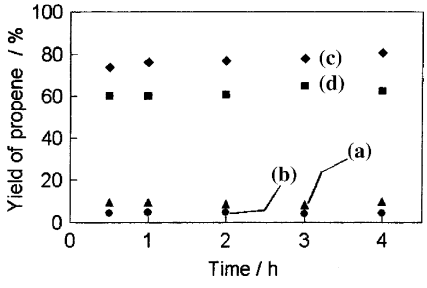

Figure 6. Catalytic activity of the dehydration of 2-propanol over supermicroporous niobium oxide (a, c) and $Nb_2O_5{\cdot}nH_2O$ (b, d). Pretreatment and reaction temperatures are as follows: (a) 200°C, (b) 200 °C, (c) 250 °C and (d) 250 °C.

that over $Nb_2O_5{\cdot}nH_2O$, yet only 20% higher at 250 °C. TEM observation of the supermicroporous niobium oxide treated at 250 °C for 4 h (the same condition as that for the reaction) finds that the original porosity of the supermicroporous niobium oxide is maintained as shown in figure 7.

The catalytic activity is usually closely related to the BET surface area. Table 3 shows relationship between pretreatment temperatures and BET surface areas. The surface area of supermicroporous niobium oxide is about twice that of $Nb_2O_5{\cdot}nH_2O$ when treated at 200 °C, implying that supermicroporous niobium oxide contains approximately twice as many active sites as the $Nb_2O_5{\cdot}nH_2O$. This fact is in good agreement with the catalytic activities of different samples at 200 °C. At 250 °C, however, the activity of supermicroporous niobium oxide is only 20% higher than that of $Nb_2O_5{\cdot}nH_2O$, even though the BET surface is still more than twice as large. This indicates that the surface area is not the only factor governing the catalytic activity in the present materials and reaction. The presence of water is regarded as an important condition for the present catalysis, and the amount of water drastically decreases at higher temperatures. Thus, the amount of active sites is not directly related to the BET surface area.

While the selectivity for propene was 100% over both catalysts at 200 °C, the selectivity of supermicroporous niobium oxide dropped to 98% at 250 °C, and was accompanied by the production of diisopropyl ether. This ether is produced via a scheme that involves a nucleophilic and an electrophilic species [11]. The formation of two products is permitted when species produced by alcohol (Lewis base) chemisorption onto

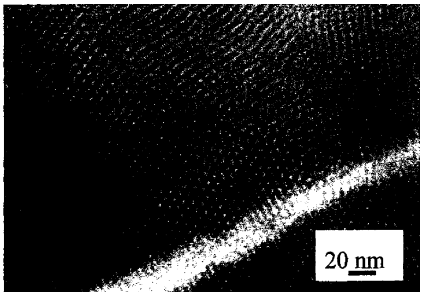

Figure 7. TEM image of supermicroporous niobium oxide calcined at 250 °C for 4 h.

Table 3
BET surface areas of the different samples treated at various temperatures ($m^2\ g^{-1}$)

Sample	Pretreatment temperature				
	50 °C	150 °C	200 °C	250 °C	300 °C
Supermicroporous niobium oxide	389	348	287	288	288
$Nb_2O_5{\cdot}nH_2O$	104	135	163	120	114

unsaturated sites (Lewis acid) and those adsorbed onto Brönsted acid sites coexist. One of the adsorbed alcohol molecules is converted into an electrophile specie, and the other develops as a leaving group, leading to dehydration. Infrared spectroscopy of adsorbed pyridine for $Nb_2O_5{\cdot}nH_2O$ revealed that $Nb_2O_5{\cdot}nH_2O$ contains both Brönsted and Lewis acid sites on the surface, and that the acidity of the respective sites is strongest when evacuated at 100 or 300 °C, respectively [12]. Thus, it is considered that Lewis acid sites in supermicroporous niobium oxide appear at lower temperatures than in $Nb_2O_5{\cdot}nH_2O$, which is probably the cause of the decrease in selectivity of propene over supermicroporous niobium oxide at 250 °C.

3.3.2. *Liquid-phase esterification of acetic acid with ethanol*

Liquid-phase reaction was tested via the esterification of acetic acid with ethanol (figure 8). Supermicroporous niobium oxides pretreated at 80 and 150 °C were compared with $Nb_2O_5{\cdot}nH_2O$ pretreated at 150 °C. Both of the supermicroporous niobium oxide samples exhibited lower activity than $Nb_2O_5{\cdot}nH_2O$, and the activities were in fact almost the same as the blank test with no catalyst.

The negligible of catalytic activity of supermicroporous niobium oxide in this reaction could not be predicted from the results of dehydration of 2-propanol and indicator adsorption, and is considered to be due not to the catalytic activity but to the reaction conditions. The diffusion rates of reactants, the solvent and the product in supermicropores may be relatively slow in the liquid-phase reactions. The same esterification was further investigated in the gas phase to confirm this observation.

3.3.3. *Gas-phase esterification of acetic acid with ethanol*

The results of esterification of acetic acid with ethanol at 160 °C in the gas phase are shown in figure 9.

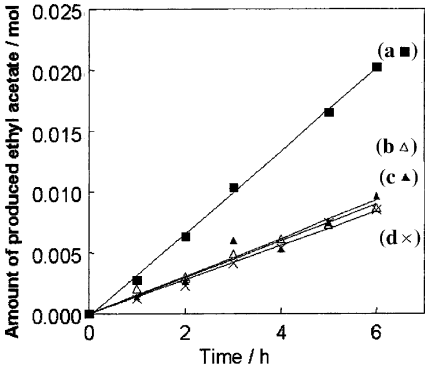

Figure 8. Catalytic activity of catalysts for liquid phase eseterification of acetic acid with ethanol: $Nb_2O_5{\cdot}nH_2O$ treated at 150 °C (a), supermicroporous niobium oxide treated at 80 °C (b), supermicroporous niobium oxide treated at 150 °C (c) and no catalyst (d).

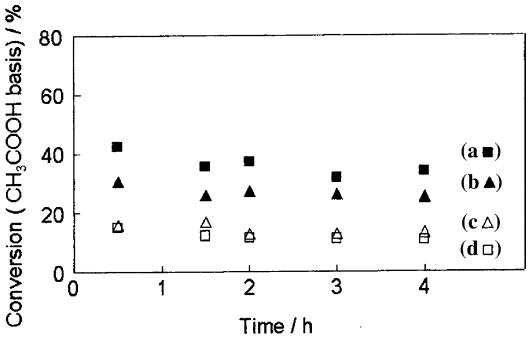

Figure 9. Catalytic activity of catalysts for gas phase esterification of acetic acid with ethanol at 160 °C: supermicroporous niobium oxide treated at 160 °C (a), supermicroporous niobium oxide treated at 200 °C (b), $Nb_2O_5{\cdot}nH_2O$ treated at 200 °C (c) and $Nb_2O_5{\cdot}nH_2O$ treated at 160 °C (d).

$Nb_2O_5{\cdot}nH_2O$ samples pretreated at 160 and 200 °C gave almost the same conversion of ethanol, and the corresponding supermicroporous niobium oxide samples produced higher rates of conversion, attributable to the greater surface area of the supermicroporous structure (table 3). The change in surface area of the supermicroporous niobium oxide samples due to pretreatment at different temperatures also explains the observed variation in activity. As shown in table 3, as the pretreatment temperature of supermicroporous niobium oxide increases, the BET surface area decreases. Thus, lower pretreatment temperature is favorable for this reaction. In all cases, the selectivity for ethyl acetate was 100%.

These results indicate that the rate of diffusion appears to be critical for reactions in porous environments at the pore sizes of the supermicroporous sample prepared here (1.5–2.5 nm pore diameter).

4. Conclusions

Supermicroporous niobium oxide was prepared by a neutral block copolymer templating route. Water washing for template removal after a second aging step afforded a highly hydrated, microporous material suitable for acid catalysis. Although the activity of this material is lower than that of $Nb_2O_5{\cdot}nH_2O$ for liquid-phase reaction, the gas-phase activities are much higher. Supermicroporous niobium oxide prepared by the present method therefore represents a suitable material for various acid-catalyzed reactions in the gas phase.

Acknowledgments

This work was supported by the Core Research for Evolutional Science and Technology (CREST) program of the Japan Science and Technology Corporation (JST).

References

[1] Z. Chen, T. Izuka and K. Tanabe, Chem. Lett. (1984) 1085.
[2] T. Hanaoka, K. Takeuchi, T. Matsuzaki and Y. Sugi, Catal. Today 8 (1990) 123.
[3] K. Ogasawara, T. Iizuka and K. Tanabe, Chem. Lett. (1984) 645.
[4] T. Yamaguchi and C. Nishimachi, Catal. Today 16 (1993) 555.
[5] K. Tanabe, Catal. Today 78 (2003) 65.
[6] B. Lee, D. Lu, J.N. Kondo and K. Domen, J. Am. Chem. Soc. 124 (2002) 11256.
[7] B. Lee, D. Lu, J.N. Kondo and K. Domen, Chem. Lett. (2002) 1058.
[8] P. Yang, D. Zhao, D.I. Margolese, B.F. Chmelka and G.D. Stucky, Nature 396 (1998) 157.
[9] P. Yang, D. Zhao, D.I. Margolese, B.F. Chmelka and G.D. Stucky, Chem. Mater. 11 (1999) 2813.
[10] S.J. Gregg and K.S.W. Sing, *Powder Surface Area and Porosity 2 nd ed.*, (Academic Press, 1970), p. 138.
[10] S.J. Gregg and K.S.W. Sing, Powder Surface Area and Porosity 2 nd ed., (Academic Press, 1970), p. 138.
[11] S. Buchang and H.D. Burtron, J. Catal. 157 (1995) 359.
[12] T. Iizuka, K. Ogasawara and K. Tanabe, Bull. Chem. Soc. Jpn. 56 (1983) 292.